Journal Pre-proof

RiMARS: An automated river morphodynamics analysis method based on remote sensing multispectral datasets

Abolfazl Jalali Shahrood, Meseret Walle Menberu, Hamid Darabi, Omid Rahmati, Pekka Rossi, Bjørn Kløve, Ali Torabi Haghighi

PII: S0048-9697(20)30846-9

DOI: https://doi.org/10.1016/j.scitotenv.2020.137336

Reference: STOTEN 137336

To appear in: *Science of the Total Environment*

Received date: 8 November 2019

Revised date: 30 January 2020

Accepted date: 14 February 2020

Please cite this article as: A.J. Shahrood, M.W. Menberu, H. Darabi, et al., RiMARS: An automated river morphodynamics analysis method based on remote sensing multispectral datasets, *Science of the Total Environment* (2018), https://doi.org/10.1016/j.scitotenv.2020.137336

RiMARS: An Automated River Morphodynamics Analysis Method Based on Remote Sensing Multispectral Datasets

Abolfazl Jalali Shahrood[1*], Meseret Walle Menberu[1], Hamid Darabi[1], Omid Rahmati[2], Pekka Rossi[1], Bjørn Kløve[1], Ali Torabi Haghighi[1]

[1]Water, Energy and Environmental Engineering Research Unit, University of Oulu, Oulu, Finland
[2]Research Center of Natural Resources and Agriculture, Institute of Watershed Management (IWM), AREEO, Kurdistan, Sanandaj 6616936311, Iran

[*]Correspondence: abolfazl.jalalishahrood@oulu.fi; a.jalali.civil@gmail.com

Abstract

Assessment and monitoring of river morphology own an important role in river engineering; since, changes in river morphology including erosion and sedimentation affect river cross-sections and flow processes. An approach for River Morphodynamics Analysis based on Remote Sensing (RiMARS) was developed and tested on the case of Mollasadra dam construction on the Kor River, Iran. Landsat multispectral images obtained from the open USGS dataset are used to extract river morphology dynamics by the Modified Normalized Difference Water Index (MNDWI). RiMARS comes with a river extraction module which is independent of threshold segmentation methods to produce binary-level images. In addition, RiMARS is equipped with developed indices for assessing the morphological alterations. Five characteristics of river morphology (spatiotemporal Sinuosity Index (SI), Absolute Centerline Migration (ACM), Rate of Centerline Migration (RCM), River Linear Pattern (RLP), and Meander Migration Index (MMI)), are applied to quantify river morphology changes. The results indicated that the Kor River centerline underwent average annual migration of 40 cm to the southwest during 1993-2003 (pre-construction impact), 20 cm to the northeast during 2003-2011, and 40 cm to the south-west during 2011-2017 (post-construction impact). Spatially, as the Kor River runs towards the Doroudzan dam, changes in river morphology have increased from upstream to downstream; particularly evident where the river flows in a plain instead of the valley. Based on SI values, there was a 5% change in

the straight sinuosity class in the pre-construction period, but an 18% decrease in the straight class during the post-construction period. Here we demonstrate the application of RiMARS in assessing the impact of dam construction on morphometric processes in Kor River, but it can be used to assess other riverine changes, including tracking the unauthorized water consumption using diverted canals. RiMARS can be applied on multispectral images.

Keywords: Environmental Monitoring**;** Iran**;** Landsat; MNDWI; Multispectral image; RiMARS; River migration; Sediments; Sinuosity Index.

1. Introduction

River morphology, sediment erosion, and accumulation are important driving factors for in-stream habitat conditions (Yang et al., 1999). Alterations in the morphology of fluvial systems can negatively affect the downstream environment, with subsequent ecological consequences such as habitat loss, disconnection of aquatic and terrestrial ecosystems (Grabowski et al., 2014), and negative effects on the diversity and composition of invertebrate populations (Choi et al., 2005). Additionally, morphological changes in rivers have socio-economic impacts on people living alongside rivers (Sear, 1994).

Fluvial systems are sensitive to climate, land, and water use changes (Heyvaert and Baeteman, 2008; Brierley et al., 2005; Heyvaert et al., 2012). Anthropogenic disturbance e.g. land use and land cover change, river modification as well as climate change are influential on major characteristics of flow regime in river (Ashraf et al., 2018; Hekmatzadeh et al. 2020; Mustonen et al., 2016; Pirnia et al., 2019; Torabi Haghighi et al., 2019; Yaraghi et al., 2019). Dams are considered to cause major anthropogenic disturbance in riverine systems, by altering the sediment yield and flow regime characteristics such as variability, magnitude, timing, and frequency (Torabi Haghighi et al., 2014; Yang et al., 2015). The impacts of dams on river morphology are well documented, e.g., it has been shown that the Garrison and Oahe

dams influence the morphological dynamics of the Upper Missouri River (Skalak et al., 2013), that the morpho-dynamics of Dry Creek stream have been considerably altered by operation of Warm Springs dam (Gordon and Meentemeyer, 2006), and that operation of Jackson Lake dam has changed the downstream channel morphological characteristics of the Snake River (Nelson et al., 2013).

Monitoring morphological alterations to fluvial systems could help manage rivers and decrease the expected impact (Darabi et al., 2019). Assessment of current morphological conditions and identification of potential alterations in the future are possible through knowledge and understanding of previous changes in river morphology (Smith and Pain, 2009). Parameters of morphological characteristics, including Sinuosity Index (SI) (Mueller, 1968; Osborne et al., 2012) average channel width (W), and flow length (L) (Yousefi et al., 2016), can be used in quantification of morphological alterations in rivers, but several different parameters are required for better understanding and analysis of river migrations. In addition, considering the length, depth, and vegetation cover of the rivers, any local assessment of geomorphological alterations is likely to be costly and time-consuming. Using new techniques such as Remote Sensing (RS) analysis could help in addressing these issues.

RS is known as an alternative to the costly and time-consuming efforts such as surveying; especially for large scale monitoring and studying morphological changes in rivers. Its reliability and effectiveness in this regard has been demonstrated in the Pearl (Zhang et al., 2015), Manu (Deb et al., 2012), Jamuna (Uddin, K., Shrestha, B., Alam, 2011), Ganga (Gupta et al., 2013), and Zambezi (Ronco et al., 2010) rivers. Water body extraction methods commonly applied using RS data are automated classification and spectral feature analysis (Guo et al., 2017). Both supervised and unsupervised automated classification algorithms have been used by several authors (Boruah et al., 2008; Gilvear et al., 2004; Wright et al., 2000) to classify different objects in the image by categorizing the pixels. Spectral feature

analysis methods have been automated recently and several attempts have been made regarding river planform extraction and quantification of meander morpho-dynamics from multispectral, grayscale, or binary-level images, including RivMAP (Schwenk, 2019), PyRIS (Monegaglia et al., 2018), RivaMap (Isikdogan et al., 2017), and SCREAM (Rowland et al., 2016). RivaMAP and PyRIS work with multispectral images while RivMAP and SCREAM packages calculate the morphological characteristics on binary masks provided by the user. RiMARS development was inspired and motivated by the similar efforts mentioned above. It seemed that the combination of extraction modules and morphological analysis in an integrated package is missing. Although PyRIS includes the morphological assessment of the rivers as well as its river path extraction features, RiMARS is equipped with several indices where migration rates of the river centerline are evaluated. Additionally, RiMARS is able to locate the meanders in a reach.

The aim of the present study was to develop an automated software package in MATLAB for River Morphodynamics Analysis based on RS data (RiMARS). Detecting and extracting the river centerline and using several indices for assessing the morphological alterations are the objectives of this study (Shahrood, 2018). To this end, we employed different indices to support the existing SI in better characterization of spatial morphological changes in rivers. A 40-km stretch of the Kor River with the average width of 100 m in southern Iran was selected as a case study to test the RiMARS software package. The selected stretch of the river is located between two dams (Mollasadra upstream and Doroudzan downstream). The impact of flow regime alteration due to Mollasadra dam construction on river morphology is investigated. At the end, the extraction module of RiMARS has been compared with two existing packages (i.e. RivaMAP and PyRIS).

2. Material and methods

2.1. Study area

The Kor River (Fig. 1), located in Lake Bakhtegan basin (Torabi Haghighi and Kløve, 2017), is one of the most important sources of freshwater in Fars province, Iran (Torabi Haghighi and Kløve, 2016). It originates from the Zagros Mountains (altitude 3600 m a.s.l.) and later joins the Sivand River at Polkhan Bridge and flows over the Korbal plain, finally discharging into the Lake Bakhtegan. The Kor River is regulated by two storage dams, Mollasadra (0.44 km^3, 2006) and Doroudzan (0.993 km^3, 1972) (Torabi Haghighi and Kløve, 2015). In this study, we focused on morphological alterations in the Kor after construction of the Mollasadra Dam in 2006. The stretch studied extended from Ab-Mahi village below the Mollasadra dam to the highest water level of the Doroudzan dam (Fig. 1b). The impact of the construction of Mollasadra dam was determined by studying changes in river morphology in pre-construction and post-construction periods. The results were compared against data from the Chamriz flow gauge record, which clearly show the impact of dam construction and possible climate-related alterations in the monthly flow regime of the Kor River downstream of the Mollasadra dam (Fig. 1c). The monthly flow data from the Chamriz gauge were considered in Landsat image selection for the study (Water Resources Atlas Report, 2011).

Fig. 1. SOMEWHERE HERE

2.2. Remote Sensing Data

Multispectral images from the Landsat archive were downloaded and used in this study. Preliminary investigations were found to be necessary to ensure the suitability of the images. Image selection was based on hydrological conditions (in order to distinguish water bodies along the river), cloud cover, and the specific date on which the image was acquired.

Temporal river morphological alterations were assessed by comparing morphological river characteristics in the pre- and post-construction periods. We selected two images from before and two from after dam construction in 2006. These consisted of Landsat 5 (TM) images

acquired in 1993, 2003, and 2011, and Landsat 8 (OLI) images acquired in 2017. The images from 1993 and 2003 represented the pre-construction period and those from 2011 and 2017 the post-construction period. Modified Normalized Difference Water Index (MNDWI) was used to produce grayscale scenes and the images selected were for periods in which large flows occurred, in order to ensure that the images showed a clear and distinct river centerline during image processing. The acquired Landsat images for 29/05/1993, 30/03/2003, 28/03/2011, and 28/03/2017 were chosen for analysis, since observed flow at the Chamriz flow gauge on these dates was considerably higher than mean flow (24 m^3s^{-1}), the daily flow in selected days were 32.42, 86.4, 30.4 and 75 m^3s^{-1} respectively. The images had a resolution of 30 m and completely covered the study area, with path and row of 163 and 39, respectively. Reflectance calibrated images were downloaded through ESPA (https://espa.cr.usgs.gov/), which is a free access portal. Morphological characteristics were assessed by considering 1993 as the reference year.

2.3 Methodology

The river morphological alteration framework developed in this study is shown in Fig. 2. MNDWI (Xu, 2006) was applied to the Landsat images for delineation of the pixels representing water as:

$$MNDWI = \frac{X_{Green} - X_{MIR}}{X_{Green} + X_{MIR}} \quad (1)$$

where X is the reflectance value of each pixel in the Green and MIR bands in a Landsat image. After extracting the river centerline by image processing, morphological alterations in the river were assessed using five different indices. These quantified either changes in river

position (Absolute Centerline Migration (ACM), Rate of Centerline Migration (RCM), and River Linear Pattern (RLP), or changes in local meander (SI and Meander Migration Index (MMI)) (Fig. 2).

Fig. 2. SOMEWHERE HERE

2.3.1. River Centerline Extraction

The river centerline was delineated in three main steps: MNDWI application, screening, and Gap-filling (Fig. 2). Each image collected from Landsat is arranged in an *m* x *n* matrix of pixels and MNDWI values for each pixel were calculated using Equation 1. This results in a grayscale image with values ranging between -1 and +1. Any threshold can be applied for producing a binary-level matrix that contains water and non-water pixels, but the procedure does not depend on threshold segmentation methods since the script is bounded to extract points in a buffer zone. The buffer zone is established by setting a polygon around the river to limit the area in which the script finds the river, e.g., the study area can be demarcated by an external prefabricated polygon that is structured through *visual interpretation* of the user in drawing programs (e.g., ArcMap). This step is not mandatory, but it is highly recommended, since the method is based on subtraction of so-called obtrusive pixels which represent moisture, but they do not exist in our region of interest. Thus, no matter which threshold is applied to the grayscale image, the script extracts the river centerline in an iterative procedure.

In RiMARS, the maximum values of MNDWI in each row and column of the matrix are assumed to represent the points of the river centerline in the screening step (the rest of points will be removed at this step). This step results in an initial layout of the river representing the centerline, but with considerable void spaces (gaps) between points.

To obtain a clearer river centerline, the screening step is followed by a Gap-filling step. Gap filling regenerates new points and inserts them inside the river in an iterative process. In the first step, the distance between each two subsequent points (gathered from screening step) is calculated by using Equation 2:

$$L = \sqrt{(x_{i+1} - x_i)^2 + (y_{i+1} - y_i)^2} \quad (2)$$

Where *L* is the direct distance between two given points, *x* and *y* are coordinates of the points.

The biggest gap between two subsequent points will be recognized (e.g. A and B in Fig. 3a) and the first point (point A) will be selected. The Gap-filling algorithm proceeds to create a *selection zone* made up by four corners (red crosses in Fig. 3b). The distance between crosses and the selected point is 70 m (due to the resolution of Landsat image 30x30 m, therefore, there would be at least two points in each side of the selected point). The points from the grayscale matrix which were removed during the screening step are brought into the selection zone (Fig. 3b and 3c). Finally, the point containing the maximum MNDWI value among other points in the selection zone is chosen as new point for river centerline (green circle in Fig. 3). The Gap-filling algorithm returns to the first step until all the gaps are not greater than 30 m (Fig. 3d, 3e and 3f).

Fig. 3. SOMEWHERE HERE

This procedure enables a detailed shape of the river centerline to be extracted. The whole process is shown in Fig. 4, where the Landsat image obtained from ESPA (Fig. 4a) is transformed to a grayscale image by applying MNDWI (Fig. 4b), and the grayscale image is transformed to a binary-level image by applying an arbitrary threshold to produce the water and non-water pixels (Fig. 4c). With the aid of the binary-level matrix and a prefabricated

polygon around the river location, the screening phase separates water pixels from non-water pixels to create an initial shape of the river centerline (Fig. 4d). Finally, the Gap-filling process fills the gaps in an iterative procedure to completely extract the river centerline (Fig. 4e). The location of the centerline points relative to the river channel can be seen in Fig. 4f.

Fig. 4. SOMEWHERE HERE

2.3.2. Linear Pattern of the River

To use the temporal centerline migration indices, we need to generate a grid based on the River Linear Pattern (RLP) (Fig. 5). RLP is a first-order linear fit (called reference line) that is applied to the points of the river centerline (results of Gap-filling in section 2.3.1) in the reference year (here 1993, black line in Fig. 5). To develop the grid, two lines (blue lines in Fig. 5, parallel to the reference line) accompanying with the series of perpendiculars (cyan lines in Fig. 5) are created. By circumscribing the grid on the river centerline, the location of intersections of river with cyan lines will be obtained in each year (Fig. 5).

Fig. 5. SOMEWHERE HERE

2.3.2.1. River Morphology Alteration Indices

To assess the changes in different parts of the river quantitatively, three indices are used in this study. These are River Linear Pattern (RLP), Absolute Centerline Migration (ACM), and Rate of Centerline Migration (RCM). River Linear Pattern is obtained by dividing a river into smaller parts (in this study five parts, each 20% (8 km) of the 40-km river stretch) and applying a first-order linear fit to each part in each year to assess the location of alterations

visually. By overlaying these fitted lines during the different years, it is possible to demonstrate alterations in each part of the river.

Absolute Centerline Migration (ACM) is a means of measuring the migrations of the river centerline in each year and compare it against that in the reference year (i.e. 1993). The mean difference between the distance of intersection points of each year (explained in previous section) and reference year is calculated for every 10% (decile) of the river length (Equation 4). Rate of Centerline Migration (RCM) is calculated using Equation 5 to evaluate the extent by which the river centerline has migrated in each period (Fig. 6).

$$ACM = \frac{\sum_{i=1}^{n}(|L_{2i}|-|L_{1i}|)}{n} \quad (3)$$

$$RCM = \frac{ACM}{Year_{m+1} - Year_m} \quad (4)$$

where L_{1i} and L_{2i} are the direct distances between intersections of the two given years (e.g., 1993 and 2003, respectively) relative to the reference line, n is the number of intersections is each decile, and m is number of the year (i.e., 1993=1, 2003=2, 2011=3, 2017=4).

Fig. 6. SOMEWHERE HERE

The Kor River runs from northwest to southeast. Negative and positive signs in calculation of ACM and RCM indicate migration of the river in the southwest and northeast direction, respectively.

2.3.3. Analysis of Meanders

This section consists of the methods for analysis of the meanders of the river. Firstly, the existing Sinuosity Index (SI) is calculated for all groups of points of the river in each year. Then the SI classes are assigned to each range of SI values and the percentage of each class in the whole river stretch will be obtained. Using the percentages, an SI class distribution map will be produced. In the next step Meander Migration Index (MMI) is used to assess the migration of the meanders quantitatively.

2.3.3.1. Sinuosity Index and meandering layout of the river

In order to evaluate morphological alterations in meanders of the river, the SI is used to analyze quantitative and qualitative aspects of meanders. The SI value is calculated as:

$$SI = \frac{CL}{DL} \tag{5}$$

where CL corresponds to channel length and DL corresponds to down-valley length.

The value of CL is obtained through the cumulative summation of the direct distances between points. The value of DL is calculated by measuring the direct distance between two specific points. Therefore, the SI value for each pair of points in the river centerline is calculated. For n number of points representing the river centerline, $\sum_{i=2}^{n} \frac{i(i-1)}{2}$ leads to a large number of SI values since there are plenty of points representing the river centerline. A database comprising SI values for all points of the river centerline in each year is made. Based on the range and magnitude of the SI, meanders are classified into four groups (Table 1) (Ashour et al., 2017; Kuriqi et al., 2017; Tiwari et al., 2016). Due to the large number of

points in the present application, the SI values are defined as the percentage of each class (Table 1).

Table. 1. SOMEWHERE HERE

Using the results of SI calculation, the four major meanders are derived based on the SI values in descending order in each year (4x4=16 meanders are selected). For example, four major meanders in the reference year (here 1993) are plotted in the first four subplots and the location of the river in other years (here 2003, 2011, and 2017) is overlaid. The same is done for all years (2003, 2011, and 2017). The meander morphodynamics can be visually interpreted from the overlaid meanders.

2.3.3.2. Meander Migration Index (MMI)

To quantify the migration of meanders, a distinct parameter should be considered. In this study we used Meander Migration Index (MMI) based on the migration of the centroids of meanders (Fig. 7). Meander Migration Index treats each meander as a polygon and the location of the centroid of each polygon is calculated and compared to the same meander over the years (Equation 2). MATLAB can locate the centroid of each polygon using a simple function known as *centroid* (Kantor I, Matoušek J, 2015).

Fig. 7. SOMEWHERE HERE

2.3.4. Model Validation

Using available survey operation data gathered from Fars Regional Water Authority, the result of the extracted points is validated. Besides, the reliability of the extraction module of

RiMARS is compared with two existing packages on the same Landsat data. PyRIS and RivaMAP are employed to extract the river path from an image gathered on 28/03/2011.

3. Results

3.1 River Linear Pattern (RLP)

Initial assessment of the centerline in the 40-km stretch of the Kor River done by RiMARS (between Ab-Mahi and Doroudzan dam) revealed that the river centerline movement is increasing along this stretch (Fig. 8a). The smallest change in the river centerline was observed in upstream parts (starting position) of the river, while the maximum change was at the downstream end of the river, where it joins the Doroudzan dam (Fig. 8b). River Linear Pattern change mainly starts at the end of fourth decile of the river stretch, at a distance of 24 km from Ab-Mahi (at about 60% of the total length of the river). This is clear from the linear fits, as the direction and gradients of overlaid linear fits differ. Furthermore, considerable changes were detected at 32 km from Ab-Mahi towards Doroudzan Lake (Fig. 8b).

Fig. 8. SOMEWHERE HERE

3.2. Kor River Centerline Migration

3.2.1. Absolute Centerline Migration (ACM)

The smallest centerline migrations (less than 1 m) were observed in the third decile of the 40-km river stretch (i.e., 20-30%) in different years (Table 2). However, in the 10th decile, maximum centerline migrations of about 100 m were observed. Most meanders were spotted in the 10th decile, a part which is close to the Doroudzan dam waterline. Comparing ACM values between each year (2003, 2011, and 2017) and the reference year (1993) revealed that considerable migrations had occurred in the fourth, sixth, seventh, eighth, ninth, and 10th

decile of the river stretch studied. Over time, the migrations showed great values, e.g., the migration value in the fourth decile of the river centerline was 34.47 m during 1993-2003, while it is increased by 7.36 m and 7.88 during 1993-2011 and 1993-2017, respectively. A corresponding increase occurred in the fifth, seventh, and eighth length deciles.

Table 2. SOMEWHERE HERE

3.2.2 Rate of Centerline Migration (RCM)

RiMARS revealed that during the first period (1993-2003), the entire centerline of the Kor River moved towards the southwest by an average rate of 40 cm per year. They also revealed an average migration of 25 cm towards the northeast in the period comprising pre- and post-dam construction (2003-2011), but the migrations were not as large as in 1993-2003. During the last period studied (2011-2017), the analysis revealed that the entire river showed a migration of about 40 cm per year towards the southwest.

Furthermore, analysis of centerline migration in sections of the 40-km stretch of the river divided into deciles showed that the rate of centerline migration in the final section had changed significantly compared with the other parts. During 1993-2003 (pre-construction), in the last decile of the river stretch length, the centerline moved towards the northeast by an annual average rate of 7.49 m, while in the sixth and seventh deciles it migrated by 4.78, and 4.82 m per year, respectively, towards the southeast and in the eighth decile by 4.97 m per year towards the northeast. During 2003-2011, the centerline in the last decile of the river moved by 3.13 m per year towards the northeast. In 2011-2017, the centerline in last decile did not show any considerable migrations, but that in the fifth decile showed an average 4.56 m per year movement towards the southeast (Table 3).

Table 3. SOMEWHERE HERE

3.3. Meanders

In this step, the proportions of each SI class are calculated and the sinuosity of the river is qualitatively and quantitatively expressed. The migration of each major meander in the river is then quantified using the migration of its centroid over time.

3.3.1. Spatio-temporal distribution of meanders along the Kor River

The results revealed that in 1993, about 33% of the river length was "straight" and 39% fell into the "winding" class. The "twisty" and "meandering" classes occupied 20% and 8% of the river length, respectively. However, the SI calculation showed that in 2003, 38% and 41% of the river stretch studied was in the straight and winding class, respectively, while 16% and 5% was categorized as twisty and meandering class, respectively. In 2011, 33% of the river length was categorized as straight class, 45% as winding, 13% as twisty, and 9% as meandering. In 2017, around 16%, 55%, 18%, and 11% of the river stretch was categorized as straight, winding, twisty, and meandering class, respectively.

During 1993-2003, the river showed a 2.9% and 3.78% reduction in the meandering and twisty classes, respectively, while the winding and straight categories increased by 1.94% and 4.74%, respectively. The post-construction impact values (2011-2017) indicate that the meandering part of the river stretch increased by 28.8% after construction of Mollasadra dam, while its straightness showed a 52% reduction. On the other hand, during 2011-2017 the winding part increased by 22% and the twisty part increased by 39%. Moreover, during 1993-2003, the length of the stretch decreased by 3.25 km. However, as river straightness decreased, the length of the stretch increased by 450 m and 2 km during 2003-2011 and 2011-2017, respectively (Fig. 9).

Fig, 9. SOMEWHERE HERE

The sinuosity categories are qualitative. Fig. 10 reveals that during 1993-2003, the straight, winding, and twisty SI classes dominated. Downstream in the river stretch, the color representing the meandering class (blue) changes to a combination of winding (black) and straight (red), indicating that during 1993-2003 the proportion of meandering class decreased and those of the winding and straight classes increased. However, during 2011-2017 the proportion of meandering class increases, and the percentage of the straight class is considerably decreased, so the river shape in 2017 shows less straightness (green) than in previous years. It has higher SI values than in previous years.

Fig. 10. SOMEWHERE HERE

3.3.2. Spatiotemporal changes in major meanders

Meanders labeled A1, A3, A4, B3, B4, and C3, in Fig. 11 migrated a considerable distance (average 109, 196, 112, 130, 124, and 84 m, respectively (Table 4)) while there was no marked migration in A2, B1, C1, and D1 (average 12 m). Meanders D3 and B2, which are situated in the first half of the river stretch, also did not show any considerable migration in meanders (15 m and 48 m, respectively). In Fig. 11, most meanders (around 75% of the major meanders) were located in the second half of the river stretch.

Fig. 11. SOMEWHERE HERE

3.3.3. Meander Migration Index (MMI)

Based on Fig. 11 and Table 4, although the centroids of meander A1 in 2003, 2011, and 2017 did not show any remarkable differences (around 5 m), the distance between the centroid of

that meander in 1993 and in other years was around 190 m. Considerable migrations occurred in meander A3 over time, with the centroid of this meander having migrated by 173 m, 176 m, and 225 m during 1993-2003, 1993-2011, and 1993-2017, respectively.

During 1993-2003, the centroid of meander A4 moved by 176 m. The centroid of meander B3 moved by 206.22 during 2011-2017. The centroids of meanders B2, and D4 did not migrate significantly (Fig. 11, Table 4).

Table 4. SOMEWHERE HERE

3.3.4. Sinuosity Index values of major meanders

The SI value changed in the major meanders A1, A3, A4, B3, and D4. In a notable alteration, the A1 meander changed from to meandering to twisty due to a 70% reduction in its SI value. Moreover, the A3 and A4 meanders changed to winding from meandering and twisty, as their SI values decreased by 36% and 25%, respectively. The 17% increase in the SI value of meander C2 changed its category from winding to twisty (Table 5).

Table 5. SOMEWHERE HERE

4. Model Validation

Validation of the RiMARS could be done with two series of observed and simulated datasets while they are synchronized temporally. Generally, observed data could be obtained through surveying operation. This type of operations is rarely available in desired time (in this case, 29/05/1993, 30/03/2003, 28/03/2011, and 28/03/2017) and location (in this case, 40 km length) owing to their costly performance, unless due to a specific reason (e.g. construction of hydraulic structures, etc.). The only available observed dataset regarding this case study is the

5-km stretch of the river boundary (i.e. Kor River) that belongs to 2009 and extends from (52°7'', 30°19") to (52°9", 30°24"). Therefore, we compared our results (extracted centerline from automated framework) in the closest year to the observed data (i.e. 2011). The results showed that 92% of the extracted centerline points are placed within the observed river boundary. It is noticed that there are some uncertainties due to the time asymmetry of the simulated and observed data.

Besides, the extraction module of the RiMARS was compared with two existing packages; i.e., RivaMAP and PyRIS. All three methods were applied on the same Landsat image in 2011 (Fig .12). The results of RivaMAP revealed huge gaps between different parts of the river (Fig. 12 c, d, f), probably due to the selected threshold and the lack of water inside the river for using the MNDWI; while RiMARS was able to find the remaining points (Fig. 12 b, d, e), owing to its Gap-filling module and its independency of thresholding methods. PyRIS also was able to trace the river without having any gaps in the points (Fig. 12 a, e, f); although, in multi-thread parts of the channel, it provides a wrong river path. In multi-thread parts, the coordinates of a selected point are an average value of its left and right pixels, thus in such parts of the river, the extracted centerline has not passed through the river main corridor (Fig. 12 a2, a3, a4). In multi-thread channels, RivaMAP works better than RiMARS and PyRIS (Fig. 12 c2).

Fig. 12. SOMEWHERE HERE

In comparison with the available software packages including PyRIS, and RivaMAP, RiMARS covers a wide variety of innovation and novelties, especially, in morpho-dynamic analysis where several metrics are automated and used to assess the morphological changes

in spatiotemporal scale. It is known as an advantage in comparison with RivaMAP package so that despite its great ability for river extraction process it is not able to compute the morpho-dynamic metrics (Schwenk et al., 2017). In terms of centerline migration analysis, the construction of mesh on the extracted centerlines enables us to measure the migrations even in higher resolutions. Additionally, the independency of using threshold segmentation methods makes RiMARS more scalable in comparison with other packages. In general, each existing package has some weaknesses along with its strengths. For instance, although RivMAP and SCREAM provide the methodology of morphodynamic analysis, they strongly rely on the type of the input data. In other words, both packages perform the morphological analysis on the binary channel masks rather than digitizing the river directly from images; therefore, the user needs to provide the temporal channel masks using different computer programs; while PyRIS, RivaMAP, and RiMARS work with the multispectral images and they extract the river planform by their own in an automated manner. That means, the binary masks are produced within the package instead of a third-party application. PyRIS and RivaMAP, both use Otsu thresholding methods for creating the binary masks from the grey-scale images. The availability of the Gap-filling module in RiMARS eliminates the need of thresholding method by sketching a first layer of the river centerline in ¨Screening¨ step based on the given arbitrary threshold, and then it finds the remaining river points in Gap-filling module. Therefore, any threshold could be selected for creating the binary image. Moreover, it appears that RivaMAP can work well with the larger rivers; while RiMARS -thanks to its double-cycle extraction (i.e. screening and Gap-filling modules)- can deal with the smaller streams too. In addition to the extraction part, RiMARS comes with several developed indices that quantifies the morphometric properties of the river and its meanders. RiMARS, PyRIS, and RivaMAP rely on moisture indices (i.e. MNDWI) to produce the grey-scale image; thus, in an image with snow and mountain shadows, pixels could be mistakenly

selected as water body. PyRIS delineates the river by using three different layers of NDVI, MNDWI, and SWIR, but as discussed earlier, it still relies on the Otsu thresholding method. In terms of morphometric analysis, PyRIS calculates the migration rates and visualizes the sediment bars which is its novel features but developed indices in RiMARS can detect the meanders of the river and calculate their morphometric alterations, in addition, it is capable of analyzing the temporal centerline migration. The results of all packages heavily depend on the resolution of the images.

5. Discussion

Determining changes in river morphology and in channel forms is a fundamental issue in fluvial geomorphology (Ahnert et al., 1965). However, assessing these changes by field surveys in natural channels is time-consuming and costly. Using RS techniques to extract geometric data can reduce the need for field surveys, leading to a significant reduction in the cost and time. In addition, poor travel links, and political limitations may increase the cost of a field survey operation that can be reduced while using RS data (Osborne et al., 2012).

The availability of Landsat data from 1972-present makes it possible to monitor and identify historical trends and employ them in future decision-making tasks. However, RiMARS is not scale-dependent and can be used for small and large rivers using any other sort of multispectral images acquired from e.g., unmanned aerial vehicles or satellite data. The process of river centerline extraction in RiMARS is performed in MATLAB, which is an improvement on the manual extraction process. Production of the binary-level images requires an optimum threshold to be used on the grayscale image obtained by applying MNDWI (Monegaglia et al., 2018; Peixoto et al., 2009; Rowland et al., 2016). However, the main advantage of RiMARS is that extraction of river centerline is independent of threshold segmentation methods. The automated process is not obliged to work with an optimum

threshold, due to its ability to search for the points of the river centerline in a repeated cycle operation. Unlike other existing software packages including PyRIS and RivaMAP, this is one of the important novel features of RiMARS that reduces the need for user intervention.

RiMARS also automates analysis of morphological characteristics by applying different indices. In comparison with RivaMAP which is well designed for extraction of the river from multispectral images RiMARS comes with several developed indices in addition to its extraction module. The employed RLP index helps identifying potential locations where changes have occurred, while the ACM and RCM indices quantify the migrations. MMI and SI are used to detect changes in meanders and their migration rates.

We used MMI as a complementary index for SI. Its benefit is illustrated by the B4 subplot in Fig. 11, where there were alterations in the meander over time. The SI results show this meander as winding, with SI values within a narrow range (Table 5), but the MMI shows that the centroid of this same meander has migrated by around 240 m, a non-negligible change. On the other hand, while the MMI results for the meander in the D4 subplot in Fig. 11 indicated only 60 m of migration, the SI value decreased from 2.06 to an average of 1.31 over time. These two indices should thus be used simultaneously, since when one index is not able to track changes, the other is likely to do so.

The results revealed that most of the migrations and morphology changes occurred in the second half of the river centerline, where the Kor River leaves a valley and suddenly expands across a plain. This allows the river to move freely, as it is not restrained by any obstacles. Therefore, as the river runs across the plain towards Doroudzan dam, the migrations become greater (Fig. 8 and Fig. 11). In addition, the migration rates show that before the construction of Mollasadra dam the alterations arose from both sedimentation and erosion, while after the

construction of the Mollasadra dam, sediment trapping occurs, and the migrations are results of only one driving factor which is erodibility.

Previous investigations have shown that since construction of the Mollasadra dam and watershed management in headwater, there have been significant decreases in sediment deposition downstream of the dam (Bagheri M., 2016, Pour et al., 2009, Seraji et al., 2009). Other studies have also found that dam construction causes a reduction in sediment discharge in downstream stretches of rivers (Lu and Siew, 2006; Richardson et al., 1975; Willis and Griggs, 2003; Xu and Milliman, 2009; Yang et al., 2006). SI shows an inverse relationship to sediment discharge (Santos-Cayado, 1973; Schumm, 1971, 1963), since "At a given valley slope, the sinuosity is in inverse proportion to the sediment load" (Petrovszki et al., 2014). This is illustrated in Fig. 9 for the stretch of the Kor River studied here, where the proportion of the meandering SI class gradually increased during the post-construction period.

There are some uncertainties resulting from limitations of RiMARS which should be manually checked. As discussed, the process of centerline extraction uses a first-order linear fit, which showed an almost perfectly fit on the Kor River centerline. In cases where the river under investigation does not follow a straight line, we recommend dividing the river into several parts and analyzing each part separately.

Moreover, in this study, the calculation of SI resulted in a few irrational values (outliers) which are not correct in reality. These outliers were removed manually to achieve better results. We also manually checked the coordinates referring to the meanders with irrational SI values and diagnosed the error that resulted in outliers. For every illogical SI value that deviated markedly from other values, we performed a manual check using the exact coordinates of the meanders and further verified by the corresponding Landsat image, to ensure that these outliers would not affect the precision of the results. It is worth mentioning

that manual checking of one of these outliers revealed the possible unauthorized water consumption by construction of diverting canals.

The 40-km length of the Kor River studied here was derived from the images provided by Landsat, which are made up of several pixels with resolution 30 m. The accuracy of methods using Landsat data is based on the resolution of the selected images (Torabi Haghighi et al., 2018). However, the migration measurements can be obtained with higher accuracy, even in centimeters; this is possible due to the process of generation of grid that intersects the river with a great deal of cross sections (Fig. 5 & 6). Furthermore, in the automated spectral feature analysis step, where the use of MNDWI is necessary for delineation of water and non-water pixels, the availability of discharge data is vital for image selection. In other words, RiMARS and other existing package which employ moisture indices such as MNDWI, are most useful for evaluating rivers with enough flow between their banks (with width of at least 30 m based on the Landsat pixel size).

To evaluate the accuracy of any modelling attempt, the error analysis could be considered. Error could arise from the resolution of the images, which is 30 m in Landsat multispectral bands. For instance, in a given reach with width of 90 m, if a pixel is mistakenly selected instead of another one, then the error is 33%. Therefore, wider rivers produce less error.

6. Conclusions

We presented RiMARS as a new method for extraction of river centerline from multispectral images and for analysis of morphological changes in rivers using RS data with the aid of MATLAB programming. We used five indices (RLP, ACM, RCM, MMI and SI) for analyzing physical characteristics and changes in river centerline and in meanders of a river. The automation of these indices help to better demonstrate river morphology changes on spatiotemporal scale, which is the main advantage of RiMARS. The automate meander

recognition module finds and classifies the major meanders in higher accuracy and shorter time than traditional methods. Additionally, a spatiotemporal feature of river layout has been presented based on classification of meanders along the river centerline.

We utilized the method on a 40-km length of the Kor River, Iran, before and after construction of the Mollasadra dam in 2006, and accuracy of the method was tested on 5 km of the river stretch using ground surveying data. It is then compared by using two existing software packages (PyRIS and RivaMAP). Application of the indices revealed detailed aspects of the morphological changes, e.g., RLP revealed that most morphological changes happened in the second half, and particularly in the last part of the river stretch, where it reaches the Doroudzan dam. ACM showed the magnitude and direction of the average centerline migration in each year, with considerable migration of around 100 m close to the Doroudzan dam that revealed the existence of Kor River in a plain is the source of huge migrations. On the other hand, migrations in the first to third deciles of the river stretch revealed that the valley in which the Kor River flows acts as a barrier that limits the magnitude of migrations (e.g. average migration 6 m). RCM index revealed that centerline migration was a function of time, e.g., in the last decile of the river stretch, the centerline migrated by 7.5 m per year before dam construction but by 0.63 m per year post-construction. Division of SI values into classes showed that after construction of Mollasadra dam, the proportion of the meandering class is gradually increased, by 2.6%, during 2011-2017, while the proportion of the straight class significantly decreased, by 17.5%. Furthermore, the results revealed the key role played by tectonic and geomorphic characteristics of the surrounding landscape (valley, plains) in changes in Kor River morphology at various spatial and temporal scales.

Although RiMARS still has some shortcomings, preliminary investigations show that it can be improved further and that it provides a way to increase the accuracy in morphological analysis by mathematical means.

7. Acknowledgements

The authors wish to express their sincere gratitude to MAA-Ja Vesitekniikan Tuki R.Y. (**MVTT** Grant no. 38616) for providing financial support to Abolfazl Jalali Shahrood to carry-out this research as part of his master's thesis at the University of Oulu in 2018. We kindly acknowledge River Engineering office of Fars Regional Water Authority and Eng. Mehrdad Tayyebi Pour for their support.

8. References

Ahnert, F., Leopold, L.B., Wolman, M.G., Miller, J.P., 1965. Fluvial Processes in Geomorphology. Geogr. Rev. 55, 452. https://doi.org/10.2307/213147

An Heyvaert, V.M., Baeteman, C., 2008. A Middle to Late Holocene avulsion history of the Euphrates river: a case study from Tell ed-Dēr, Iraq, Lower Mesopotamia. Quat. Sci. Rev. 27, 2401–2410. https://doi.org/10.1016/j.quascirev.2008.08.024

Ashour, M.A., Saad, M.S., Kotb, M.M., 2017. Evaluation of Alluvial Channels Meandering Phenomenon (Case Study: Bahr Youssef). Ann. Valahia Univ. Targoviste, Geogr. Ser. 17, 206–219. https://doi.org/10.1515/avutgs-2017-0019

Ashraf, F.B., Torabi Haghighi, A, Riml, J., Alfredsen, K., Koskela, J.J., Kløve, B., et al., 2018. Changes in short term river flow regulation and hydropeaking in Nordic rivers. Sci.Rep. 8.

Bagheri M., 2016. Investigation of Runoff and Sedimentation of the Basin Using SWAT Model, Mollasadra Dam Case Study. Marvdash Azad University.

Boruah, S., Gilvear, D.J., Hunter, P., Sharma, N., 2008. Quantifying channel planform and physical habitat dynamics on a large braided river using satellite data - The Brahmaputra, India, in: River Research and Applications. pp. 650–660. https://doi.org/10.1002/rra.1132

Brierley, G.J., Brooks, A.P., Fryirs, K., Taylor, M.P., 2005. Did humid-temperate rivers in the Old and New Worlds respond differently to clearance of riparian vegetation and removal of woody debris? Prog. Phys. Geogr. https://doi.org/10.1191/0309133305pp433ra

Choi, S.U., Yoon, B., Woo, H., 2005. Effects of dam-induced flow regime change on downstream river morphology and vegetation cover in the Hwang River, Korea. River Res. Appl. 21, 315–325. https://doi.org/10.1002/rra.849

Darabi, H., Choubin, B., Rahmati, O., Torabi Haghighi, A., Pradhan, B., Kløve, B., 2019. Urban flood risk mapping using the GARP and QUEST models: A comparative study of machine learning techniques. J. Hydrol. 569, 142–154. https://doi.org/10.1016/j.jhydrol.2018.12.002

Deb, M., Das, D., Uddin, M., 2012. Evaluation of Meandering Characteristics Using RS & GIS of Manu River. J. Water Resour. Prot. 04, 163–171. https://doi.org/10.4236/jwarp.2012.43019

Gilvear, D.J., Davids, C., Tyler, A.N., 2004. The use of remotely sensed data to detect channel hydromorphology: River Tummel, Scotland. River Res. Appl. 20, 795–811. https://doi.org/10.1002/rra.792

Gordon, E., Meentemeyer, R.K., 2006. Effects of dam operation and land use on stream channel morphology and riparian vegetation. Geomorphology 82, 412–429. https://doi.org/10.1016/j.geomorph.2006.06.001

Grabowski, R.C., Surian, N., Gurnell, A.M., 2014. Characterizing geomorphological change to support sustainable river restoration and management. Wiley Interdiscip. Rev. Water 1, 483–512. https://doi.org/10.1002/wat2.1037

Guo, Q., Pu, R., Li, J., Cheng, J., 2017. A weighted normalized difference water index for water extraction using landsat imagery. Int. J. Remote Sens. 38, 5430–5445. https://doi.org/10.1080/01431161.2017.1341667

Gupta, N., Atkinson, P.M., Carling, P.A., 2013. Decadal length changes in the fluvial planform of the River Ganga: Bringing a mega-river to life with Landsat archives. Remote Sens. Lett. 4, 1–9. https://doi.org/10.1080/2150704X.2012.682658

Hekmatzadeh, A.A., Torabi Haghighi, A., Kløve, B., 2019, The effects of extremes and temporal scale on multifractal properties of streamflow time series. River Res. Appl., 2020, 36, 1, 171-182.

Heyvaert, V.M.A., Walstra, J., Verkinderen, P., Weerts, H.J.T., Ooghe, B., 2012. The role of human interference on the channel shifting of the Karkheh River in the Lower Khuzestan plain (Mesopotamia, SW Iran). Quat. Int. 251, 52–63. https://doi.org/10.1016/j.quaint.2011.07.018

Isikdogan, F., Bovik, A., Passalacqua, P., 2017. RivaMap: An automated river analysis and mapping engine. Remote Sens. Environ. 202, 88–97. https://doi.org/10.1016/j.rse.2017.03.044

Kantor I, Matoušek J, Š.R., 2015. Mathematics.

Kuriqi, A., Rosário Fernandes, M., Santos, A., Ferreira, M.T., 2017. Historical Maps Potential on the Assessment of the Hydromorphological Changes in Large Rivers: Towards Sustainable Rivers Management under Altered Flows.

Lu, X.X., Siew, R.Y., 2006. Water discharge and sediment flux changes over the past decades in the Lower Mekong River: Possible impacts of the Chinese dams. Hydrol. Earth Syst. Sci. 10, 181–195. https://doi.org/10.5194/hess-10-181-2006

Monegaglia, F., Zolezzi, G., Güneralp, I., Henshaw, A.J., Tubino, M., 2018. Automated extraction of meandering river morphodynamics from multitemporal remotely sensed data. Environ. Model. Softw. 105, 171–186. https://doi.org/10.1016/j.envsoft.2018.03.028

Mueller, J.E., 1968. An introduction to the hydraulic AND TOPOGRAPHIC SINUOSITY INDEXES. Ann. Assoc. Am. Geogr. 58, 371–385. https://doi.org/10.1111/j.1467-8306.1968.tb00650.x

Mustonen, k.; Mykrä, H.; Marttila, H., **Torabi Haghighi, A.,** Kløve, B., Aroviita, J.; Veijalainen, N; Sippel, K; Muotka, T; 2016. Defining natural flow regimes of highly seasonal boreal rivers: relationship with taxonomical and functional structure of macroinvertebrate communities. Freshwater Science, 35.

Nelson, N.C., Erwin, S.O., Schmidt, J.C., 2013. Spatial and temporal patterns in channel change on the Snake River downstream from Jackson Lake dam, Wyoming. Geomorphology 200, 132–142. https://doi.org/10.1016/j.geomorph.2013.03.019

Osborne, B.P., Osborne, V.J., Kruger, M.L., 2012. COMPARISON OF SATELLITE SURVEYING TO TRADITIONAL 65, 98–104.

Peixoto, J.M.A., Nelson, B.W., Wittmann, F., 2009. Spatial and temporal dynamics of river channel migration and vegetation in central Amazonian white-water floodplains by remote-sensing techniques. Remote Sens. Environ. 113, 2258–2266. https://doi.org/10.1016/j.rse.2009.06.015

Petrovszki, J., Timár, G., Molnár, G., 2014. Is sinuosity a function of slope and bankfull discharge? – A case study of the meandering rivers in the Pannonian Basin. Hydrol. Earth Syst. Sci. Discuss. 11, 12271–12290. https://doi.org/10.5194/hessd-11-12271-2014

Pirnia, A., Darabi, H., Choubin, B., Omidvar, E., Onyutha, C., Haghighi, A.T., 2019. Contribution of climatic variability and human activities to stream flow changes in the Haraz River basin, northern Iran. J. Hydro-Environment Res. 25, 12–24. https://doi.org/10.1016/j.jher.2019.05.001

Pour, R.M., Haghighi, A.T., Saremi, H., Keshtkaran, P., 2009. Watershed management and its effect on sedimentation in doroudzan dam, Sichuan Daxue Xuebao (Gongcheng Kexue Ban) 41, 242-248.

Richardson, E. V, Karaki, S., Mahmood, K., Simons, D.B., Stevens, M.A., 1975. Highways in the river environment, hydraulic and environmental design considerations : training and design manual.

Ronco, P., Fasolato, G., Nones, M., Di Silvio, G., 2010. Morphological effects of damming on lower Zambezi River. Geomorphology 115, 43–55. https://doi.org/10.1016/j.geomorph.2009.09.029

Rowland, J.C., Shelef, E., Pope, P.A., Muss, J., Gangodagamage, C., Brumby, S.P., Wilson, C.J., 2016. A morphology independent methodology for quantifying planview river change and characteristics from remotely sensed imagery. Remote Sens. Environ. 184, 212–228. https://doi.org/10.1016/j.rse.2016.07.005

Santos-Cayado, J., 1973. STAGE DETERMINATION FOR HIGH DISCHARGES.

Schumm, S.A., 1971. Fluvial geomorphology: the historical perspective. River Mech.

Schumm, S.A., 1963. Sinuosity of alluvial rivers on the great plains. Bull. Geol. Soc. Am. 74, 1089–1100. https://doi.org/10.1130/0016-7606(1963)74[1089:SOAROT]2.0.CO;2

Schwenk, J., 2019. RivMAP - River Morphodynamics from Analysis of Planforms.

Schwenk, J., Khandelwal, A., Fratkin, M., Kumar, V., Foufoula-Georgiou, E., 2017. High spatiotemporal resolution of river planform dynamics from landsat: The rivMAP toolbox and results from the Ucayali river. Earth Sp. Sci. 4, 46–75. https://doi.org/10.1002/2016EA000196

Sear, D.A., 1994. River restoration and geomorphology. Aquat. Conserv. Mar. Freshw. Ecosyst. 4, 169–177. https://doi.org/10.1002/aqc.3270040207

Seraji, M.H.S., Haghighi, A.T., Keshtkaran, P., 2009. Comparing the real value of sediment load with the results of erosion models in Kor River. Sichuan Daxue Xuebao (Gongcheng Kexue Ban)/Journal of Sichuan University (Engineering Science Edition) 41, 319-324.

Shahrood, A.J., 2018. Assessing the Impacts of Dam Construction on River Morphology by Applying a New Automated Method on Remote Sensing Images. University of Oulu.

Skalak, K.J., Benthem, A.J., Schenk, E.R., Hupp, C.R., Galloway, J.M., Nustad, R.A., Wiche, G.J., 2013. Large dams and alluvial rivers in the Anthropocene: The impacts of the Garrison and Oahe Dams on the Upper Missouri River. Anthropocene 2, 51–64. https://doi.org/10.1016/j.ancene.2013.10.002

Smith, M.J., Pain, C.F., 2009. Applications of remote sensing in geomorphology. Prog. Phys. Geogr. 33, 568–582. https://doi.org/10.1177/0309133309346648

Tiwari, H., Rai, S.P., Shivangi, K., 2016. Bridging the gap or broadening the problem? Nat. Hazards 84, 351–366. https://doi.org/10.1007/s11069-016-2422-x

Torabi Haghighi, A., Darabi, H., Shahedi, K., Solaimani, K., Kløve, B., 2019. A Scenario-Based Approach for Assessing the Hydrological Impacts of Land Use and Climate Change in the Marboreh Watershed, Iran. Environ. Model. Assess. https://doi.org/10.1007/s10666-019-09665-x

Torabi Haghighi, A., Kløve, B., 2017. Design of environmental flow regimes to maintain lakes and wetlands in regions with high seasonal irrigation demand. Ecol. Eng. 100, 120–129. https://doi.org/10.1016/j.ecoleng.2016.12.015

Torabi Haghighi, A., Kløve, B., 2015. Development of monthly optimal flow regimes for allocated environmental flow considering natural flow regimes and several surface water protection targets. Ecol. Eng. 82, 390–399. https://doi.org/10.1016/j.ecoleng.2015.05.035

Torabi Haghighi, A., Marttila, H., Kløve, B., 2014. Development of a new index to assess river regime impacts after dam construction. Glob. Planet. Change 122, 186–196. https://doi.org/10.1016/j.gloplacha.2014.08.019

Torabi Haghighi, A., Menberu, M.W., Aminnezhad, M., Marttila, H., Kløve, B., 2016. Can lake sensitivity to desiccation be predicted from lake geometry? J. Hydrol. 539, 599–610. https://doi.org/10.1016/j.jhydrol.2016.05.064

Torabi Haghighi, A., Menberu, M.W., Darabi, H., Akanegbu, J., Kløve, B., 2018. Use of remote sensing to analyse peatland changes after drainage for peat extraction. L. Degrad. Dev. 29, 3479–3488. https://doi.org/10.1002/ldr.3122

Uddin, K., Shrestha, B., Alam, M.S., 2011. Assessment of morphological changes and vulnerability of river bank erosion alongside the river Jamuna using remote sensing. J. Earth Sci. Eng. 1.

Willis, C.M., Griggs, G.B., 2003. Reductions in fluvial sediment discharge by coastal dams in California and implications for beach sustainability. J. Geol. 111, 167–182. https://doi.org/10.1086/345922

Wright, A., Marcus, W.A., Aspinall, R., 2000. Evaluation of multispectral, fine scale digital imagery as a tool for mapping stream morphology. Geomorphology 33, 107–120. https://doi.org/10.1016/S0169-555X(99)00117-8

Xu, H., 2006. Modification of normalised difference water index (NDWI) to enhance open water features in remotely sensed imagery. Int. J. Remote Sens. 27, 3025–3033. https://doi.org/10.1080/01431160600589179

Xu, K., Milliman, J.D., 2009. Seasonal variations of sediment discharge from the Yangtze River before and after impoundment of the Three Gorges Dam. Geomorphology 104, 276–283. https://doi.org/10.1016/j.geomorph.2008.09.004

Yang, S.L., Xu, K.H., Milliman, J.D., Yang, H.F., Wu, C.S., 2015. Decline of Yangtze River water and sediment discharge: Impact from natural and anthropogenic changes. Sci. Rep. 5. https://doi.org/10.1038/srep12581

Yang, X., Damen, M.C.J., Van Zuidam, R.A., 1999. Satellite remote sensing and GIS for the analysis of channel migration changes in the active Yellow River Delta, China. ITC J. 1, 146–157. https://doi.org/10.1016/S0303-2434(99)85007-7

Yang, Z., Wang, H., Saito, Y., Milliman, J.D., Xu, K., Qiao, S., Shi, G., 2006. Dam impacts on the Changjiang (Yangtze) River sediment discharge to the sea: The past 55 years and after the Three Gorges Dam. Water Resour. Res. 42. https://doi.org/10.1029/2005WR003970

Yaraghi, N., Ronkanen, A., Darabi, H., Kløve, B., Torabi Haghighi, A, 2019, Impact of

Managed Aquifer Recharge on river flow regimes in arid and semi-arid climates, STOTEN. 675, 429-438. https://doi.org/10.1016/j.scitotenv.2019.04.253

Yousefi, S., Pourghasemi, H.R., Hooke, J., Navratil, O., Kidová, A., 2016. Changes in morphometric meander parameters identified on the Karoon River, Iran, using remote sensing data. Geomorphology 271, 55–64. https://doi.org/10.1016/j.geomorph.2016.07.034

Zhang, W., Xu, Y., Hoitink, A.J.F., Sassi, M.G., Zheng, J., Chen, X., Zhang, C., 2015. Morphological change in the Pearl River Delta, China. Mar. Geol. 363, 202–219. https://doi.org/10.1016/j.margeo.2015.02.012

Declaration of interests

☒ The authors declare that they have no known competing financial interests or personal relationships that could have appeared to influence the work reported in this paper.

☐The authors declare the following financial interests/personal relationships which may be considered as potential competing interests:

Fig. 1. a) Location of Lake Bakhtegan basin in Iran, and storage/diversion dams, b) Location of the study area in the Lake Bakhtegan basin, Iran, and layout of hydraulic structures, and c) monthly flow at Chamriz gauge station during pre- and post-damming periods.

Fig. 2. Flowchart of the procedure devised to assess morphological alterations in a river. MNDWI: Modified Normalized Difference Water Index, RLP: River Linear Pattern, RCM: Rate of Centerline Migration, ACM: Absolute Centerline Migration, SI: Sinuosity Index, MMI: Meander Migration Index.

Fig. 3. Gap-filling algorithm. (a): a stretch of the Kor River where the maximum distance between a pair of points is located, (b): locating the first point and regenerating the selection zone, (c): selecting the new point from the MNDWI cluster, (d): locating the next point and regenerating the selection zone, (e): selecting the new point from the MNDWI cluster (f): locating the next point and regenerating the selection zone.

Fig. 4. River centerline extraction processes, (a) False-color Landsat image (CIR), (b) grayscale image (Modified Normalized Difference Water Index, MNDWI), (c) binary-level image, (d) result of screening, (e) result of gap-filling, and (f) river channel relative to centerline points.

Fig. 5. Schematic figure of generating mesh using two parallel lines and a series of perpendicular lines. The distance of the perpendicular lines is 50 m.

Fig. 6. (a): river stretch in 1993 and 2003 and the position of the reference line, (b): the calculation of the distance between each corresponding point of the river and the reference line

Fig. 7. Schematic view of the migration of centroid of meanders. Blue and red represent the first and second locations of a specific meander, respectively.

Fig. 8. (a) Overlay of river paths in the four different years studied and (b) overlay of River Linear Pattern (RLP) in the different years for the 40-km stretch of the Kor River analyzed in this study.

Fig. 9. Summary of meander classification for the 40-km stretch of the Kor River studied here, based on Sinuosity Index (SI, %).

Fig. 10. Visualization of the different proportions of sinuosity classes in each year.

Fig. 11. Spatiotemporal comparison of major meanders during the study period, where letters A, B, C, and D represent 1993, 2003, 2011, and 2017, respectively, and the numbers 1, 2, 3, 4 represent the magnitude of meander in terms of its SI value in descending order. Each subplot shows a comparison of three meanders with one meander belonging to the respective year (i.e., A, B, C, and D).

Fig. 12. Comparison of extraction modules of existing packages including a) PyRIS, b) RiMARS, and c) RivaMAP. Visualization of the results by overlaying the outputs of d) RiMARS and RivaMAP, e) RiMARS and PyRIS, and f) RivaMAP and PyRIS.

Table 1 Sinuosity Index (SI) classification for meander analysis (Ashour et al., 2017; Kuriqi et al., 2017; Tiwari et al., 2016).

Sinuosity Class	SI Numerical Range
Straight	$SI < 1.05$
Winding	$1.05 \leq SI \leq 1.25$
Twisty	$1.25 \leq SI \leq 1.50$
Meandering	$SI \geq 1.50$

Table 2. Absolute Centerline Migration values (m) of the Kor River compared with the reference year (1993)

Spatial interval	1993-2003	1993-2011	1993-2017
Entire river	-3.92	-2	-4.34
0-10%	-4.32	1.91	11.58
10-20%	-5.14	-6.62	1.47
20-30%	**0.12**	**0.08**	**-0.7**
30-40%	**-34.47**	**-41.83**	**-49.71**
40-50%	8.13	9.09	-18.25
50-60%	-47.74	-46.53	-59.73
60-70%	-48.12	-51.24	-60.57
70-80%	49.64	63.58	71.51
80-90%	-33.71	-49.86	-36.88
90-100%	74.83	**99.86**	**96.13**

Table 3. Rate of Centerline Migration (m/year) of the Kor River in pre- and post-damming periods (dam construction in 2006)

Spatial interval	Pre-damming	Pre- and post-damming	Post-damming
	1993-2003	**2003-2011**	**2011-2017**
Entire river	-0.4	0.25	-0.39
0–10%	-0.44	0.78	1.62
10–20%	-0.52	-0.19	1.35
20–30%	0.02	-0.01	-0.13
30–40%	-3.45	-0.93	-1.32
40–50%	0.82	0.13	**-4.56**
50–60%	**-4.78**	0.16	-2.21
60–70%	**-4.82**	-0.39	-1.56
70–80%	**4.97**	1.75	1.33
80–90%	-3.38	-2.02	2.17
90–100%	**7.49**	**3.13**	-0.63

Table 4. Temporal changes in centroid migration in major meanders of the Kor River stretch studied (see Figure 10 for meander locations)

Subplot		1993-2003	1993-2011	1993-2017	2003-2011	2003-2017	2011-2017
A	1	184.3	189.68	184.13	48.59	31.19	17.61
	2	13.16	31.07	21.55	18.55	9.81	9.65
	3	173.61	176.46	**225.52**	67.49	295.07	240.23
	4	**176.55**	161.55	171.18	81.77	58.41	25.85
B	1	11.74	23.67	20.11	12.2	9.84	5.37
	2	48.66	55.19	56.14	6.97	7.61	1.44
	3	101.41	103.87	156.06	93.42	117.83	**206.21**
	4	238.53	240.85	217.4	5.03	23.76	24.37
C	1	10.26	22.7	18.52	12.97	9.77	5.07
	2	75.92	104.36	90.52	33.68	25.08	14.47
	3	33.53	77.4	145.12	45.54	114.42	92.65
	4	62.67	72.35	58.69	52.54	42.82	14.37
D	1	12.56	25.37	21.42	13.03	9.87	5.01
	2	92.55	92.48	93.84	54.26	72.99	19.5
	3	15.44	15.55	7.16	14.08	8.57	11.29
	4	61.19	33.52	55.4	28.3	15.56	22.45

Table 5. Sinuosity Index value of each major meander of the Kor River stretch studied (see Figure 10 for meander locations)

Subplot	1993	2003	2011	2017
A1	**2.12**	1.25	1.26	1.32
A2	1.91	2.06	2.16	2.14
A3	**1.50**	1.02	1.04	1.15
A4	**1.40**	1.08	1.07	1.22
B1	2.03	2.04	2.16	2.12
B2	1.32	1.51	1.55	1.60
B3	1.89	1.24	1.22	1.35
B4	1.10	1.21	1.16	1.23
C1	2.10	2.20	2.27	2.29
C2	1.11	1.13	1.33	1.30
C3	1.22	1.16	1.28	1.05
C4	1.24	1.10	1.34	1.31
D1	2.10	2.13	2.20	2.21
D2	1.33	1.12	1.24	1.46
D3	1.34	1.28	1.32	1.38
D4	**2.06**	1.24	1.29	1.41

Graphical abstract

Highlights

- River delineation process does not rely on threshold segmentation methods
- Gap-filling module iterates the point regeneration process to create the river path
- RiMARS can detect the meanders of the river
- RiMARS employed five developed indices to assess the morphological alterations
- Major Meander Index is used as a complementary alternative for Sinuosity Index

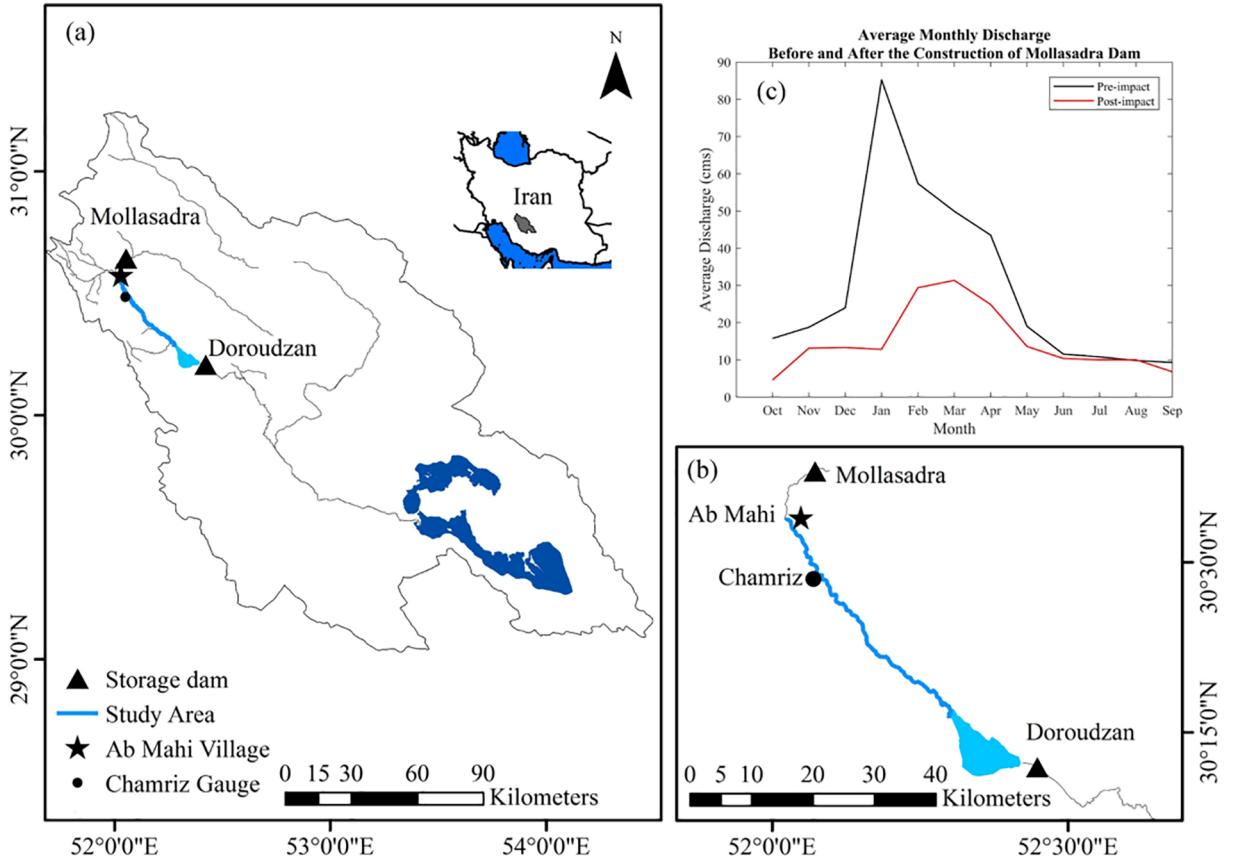
(a)
N
Iran
Mollasadra
Doroudzan
31°0'0"N
30°0'0"N
29°0'0"N
52°0'0"E
53°0'0"E
54°0'0"E
Storage dam
Study Area
Ab Mahi Village
Chamriz Gauge
0 15 30 60 90
Kilometers
Average Monthly Discharge
Before and After the Construction of Mollasadra Dam
(c)
Pre-impact
Post-impact
Average Discharge (cms)
90
80
70
60
50
40
30
20
10
0
Oct Nov Dec Jan Feb Mar Apr May Jun Jul Aug Sep
Month
(b)
Mollasadra
Ab Mahi
Chamriz
Doroudzan
0 5 10 20 30 40
Kilometers
30°30'0"N
30°15'0"N
52°0'0"E
52°30'0"E

Figure 1

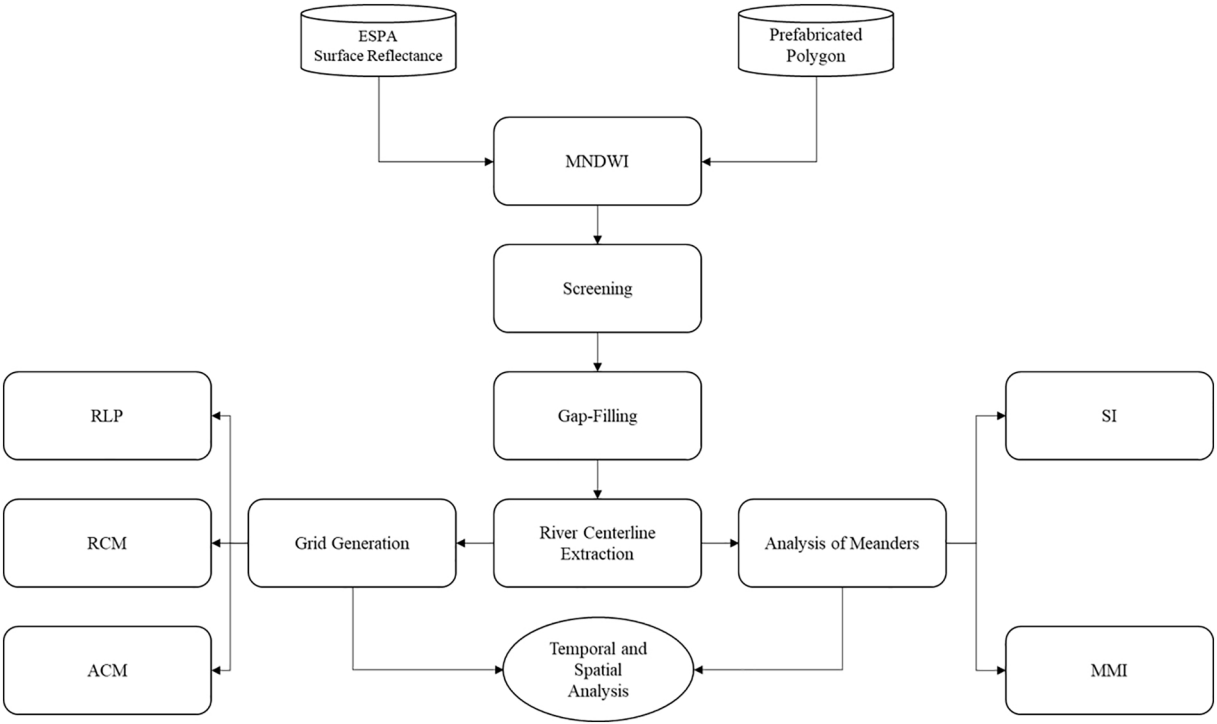
ESPA
Surface Reflectance
Prefabricated
Polygon
MNDWI
Screening
Gap-Filling
RLP
RCM
ACM
Grid Generation
River Centerline
Extraction
Analysis of Meanders
SI
MMI
Temporal and
Spatial
Analysis

Figure 2

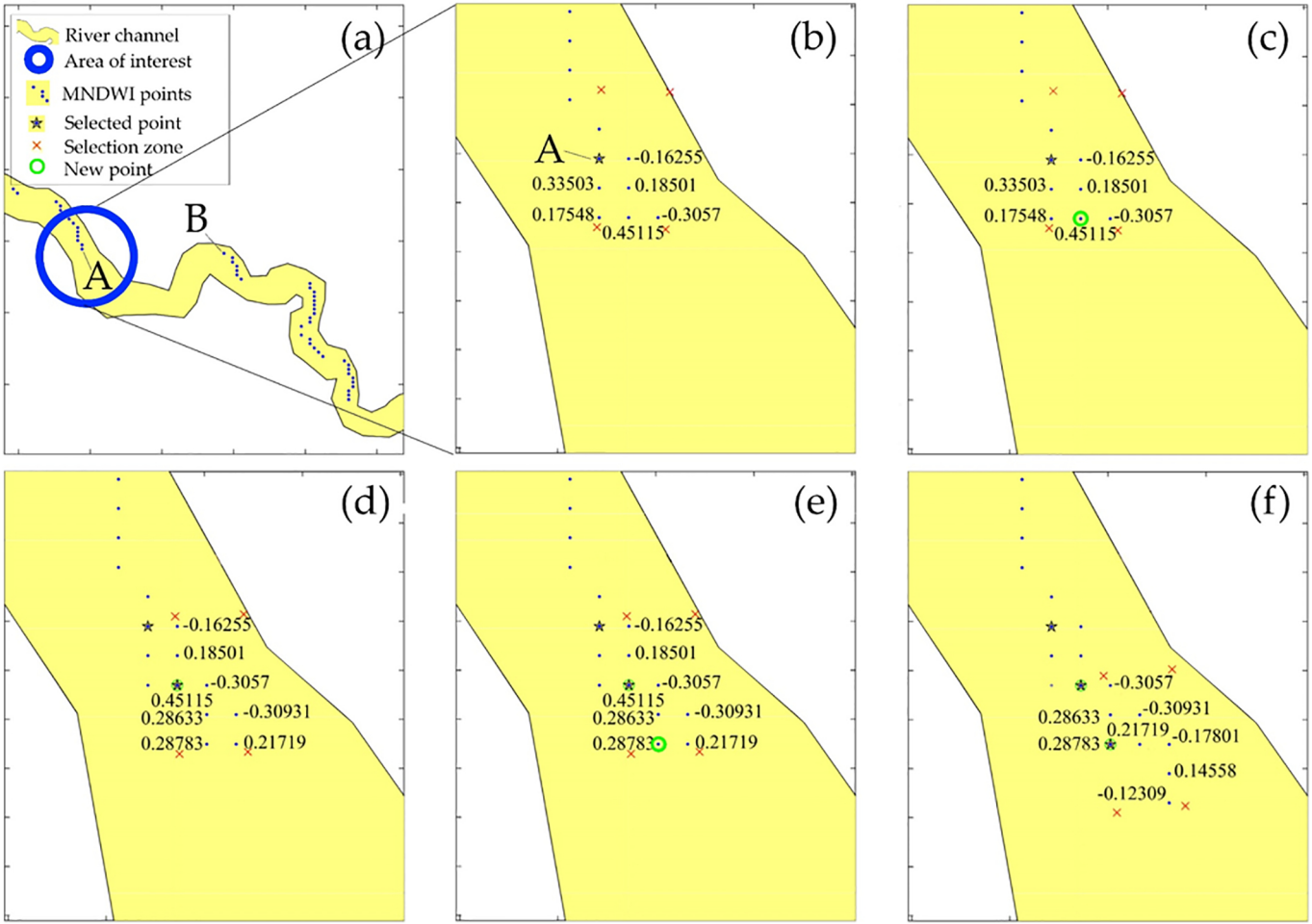
River channel
Area of interest
MNDWI points
Selected point
Selection zone
New point
(a)
A
B
(b)
A
-0.16255
0.33503
0.18501
0.17548
-0.3057
0.45115
(c)
-0.16255
0.33503
0.18501
0.17548
-0.3057
0.45115
(d)
-0.16255
0.18501
-0.3057
0.45115
0.28633
-0.30931
0.28783
0.21719
(e)
-0.16255
0.18501
-0.3057
0.45115
0.28633
-0.30931
0.28783
0.21719
(f)
-0.3057
0.28633
-0.30931
0.21719
0.28783
-0.17801
0.14558
-0.12309

Figure 3

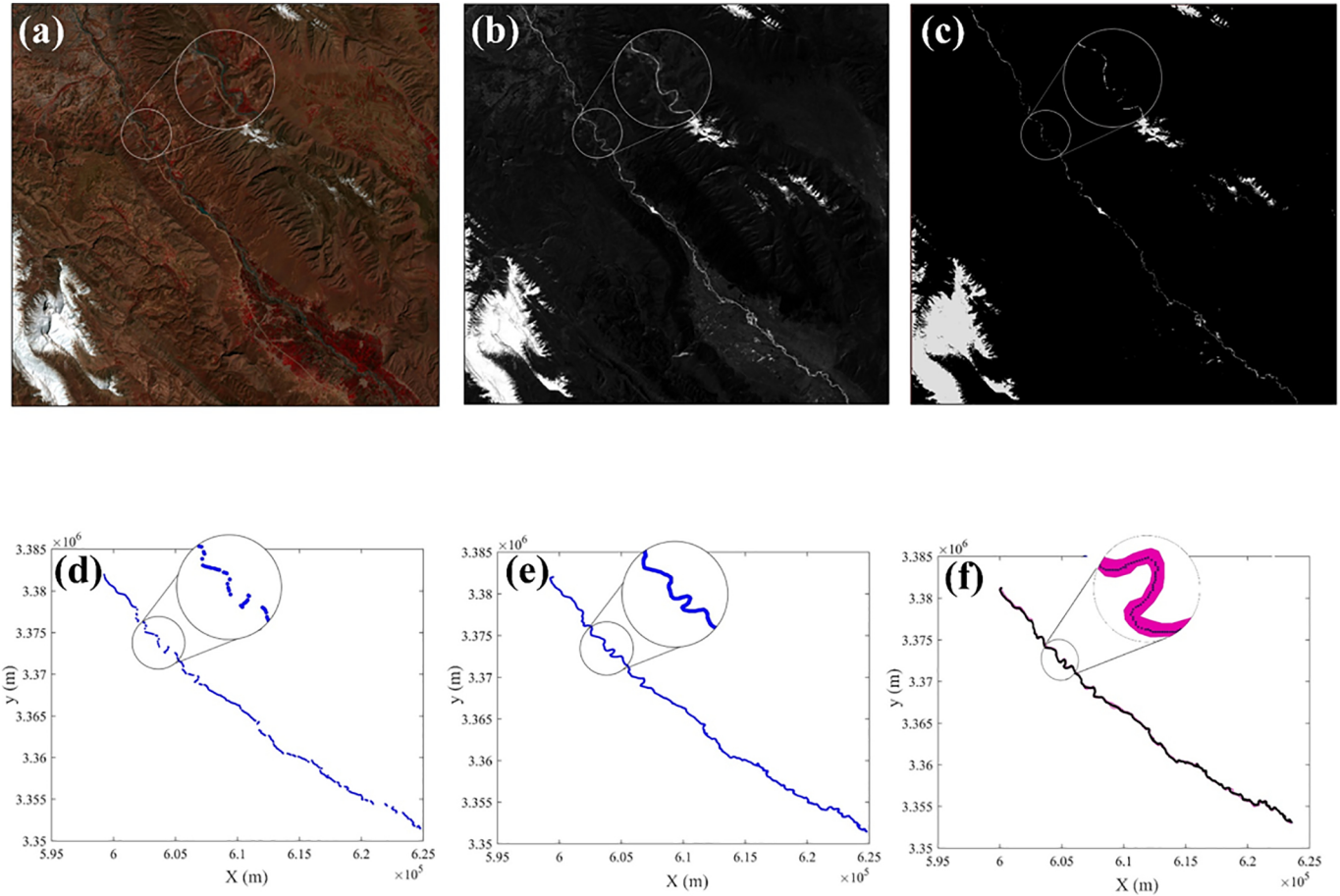
(a)
(b)
(c)
(d)
(e)
(f)
×10^6
3.385
3.38
3.375
3.37
3.365
3.36
3.355
3.35
y (m)
5.95
6
6.05
6.1
6.15
6.2
6.25
X (m)
×10^5

Figure 4

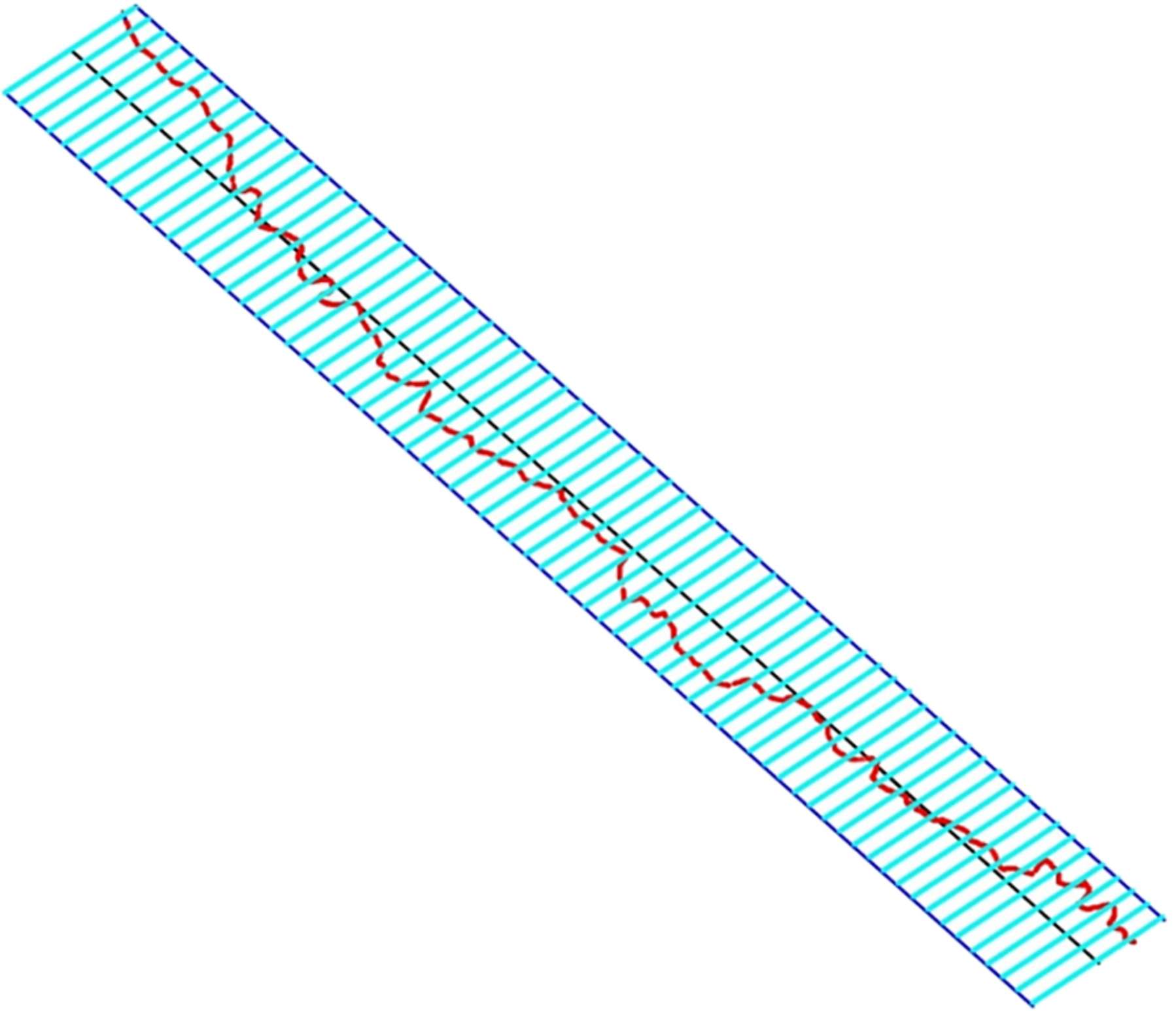

Figure 5

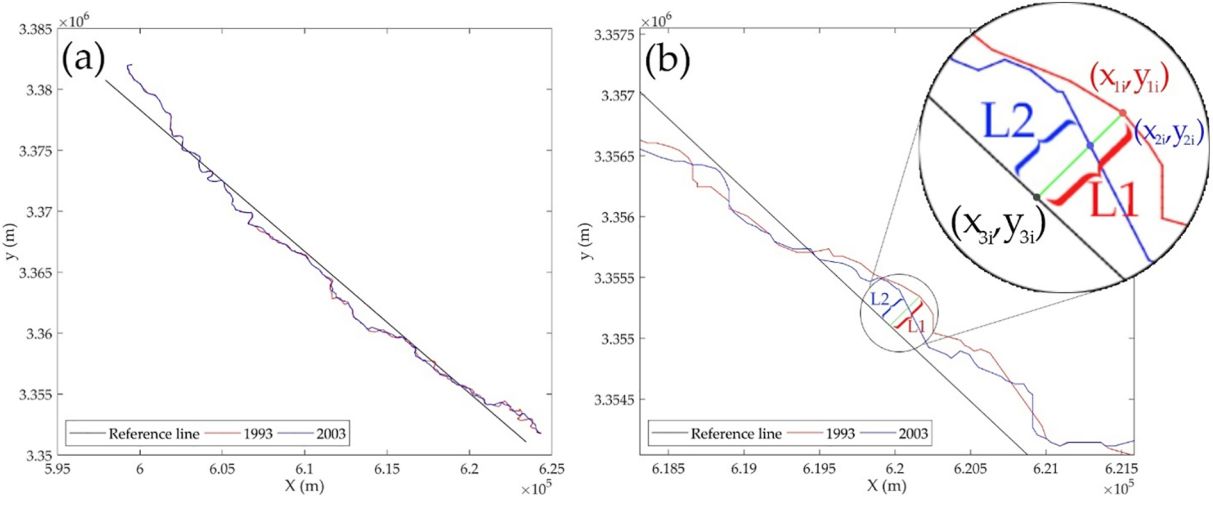
(a)
(b)
×10^6
y (m)
X (m)
×10^5
Reference line
1993
2003
L1
L2
(x1i, y1i)
(x2i, y2i)
(x3i, y3i)

Figure 6

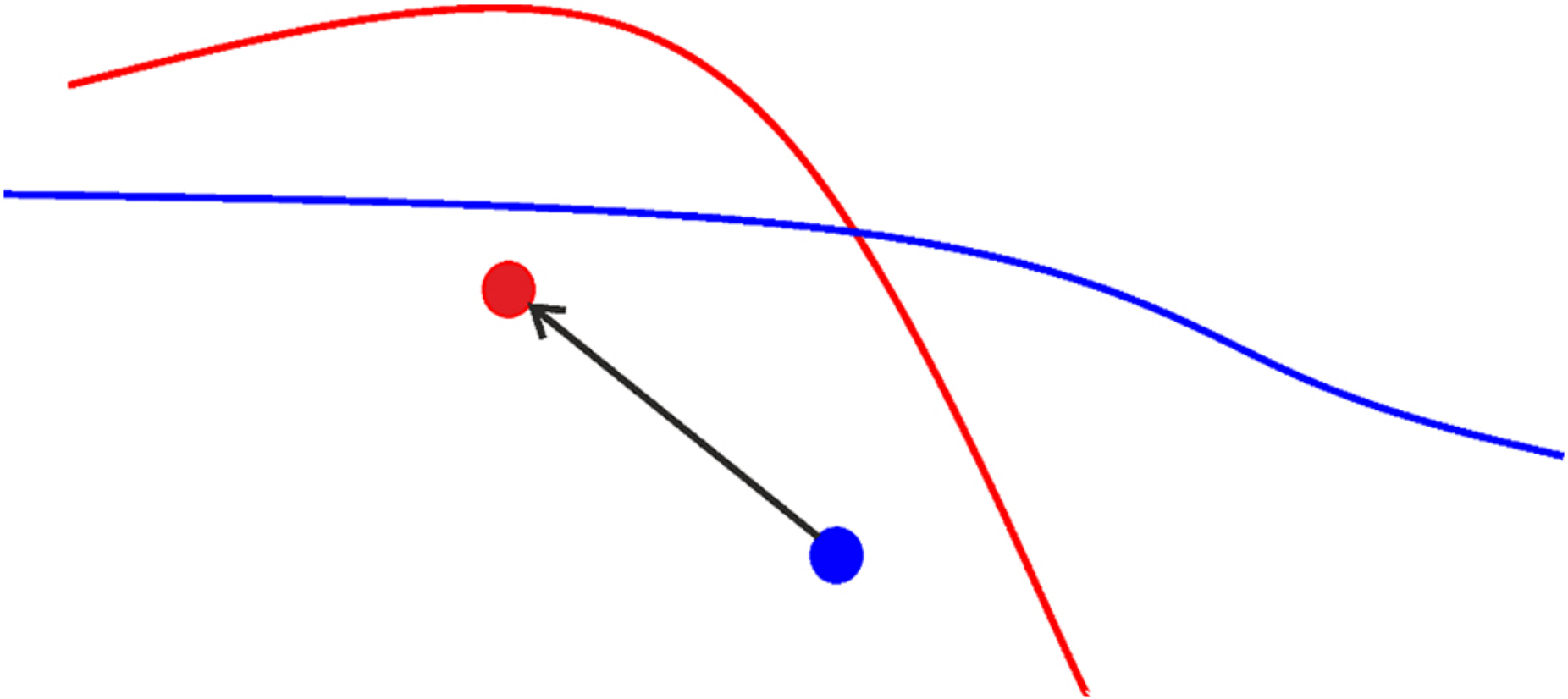

Figure 7

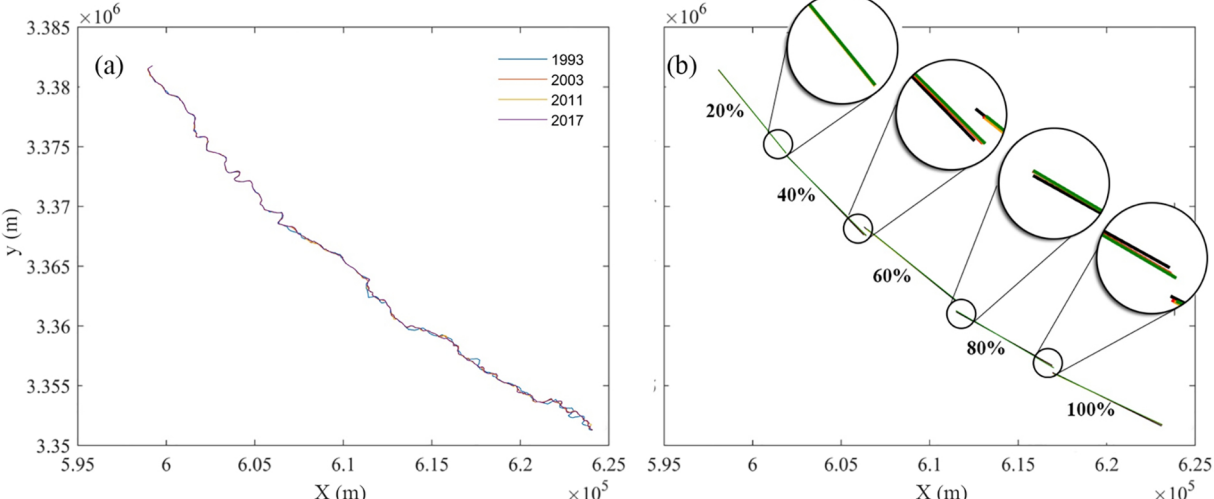
(a)
1993
2003
2011
2017
×10^6
3.385
3.38
3.375
3.37
3.365
3.36
3.355
3.35
y (m)
5.95
6
6.05
6.1
6.15
6.2
6.25
X (m)
×10^5
(b)
×10^6
20%
40%
60%
80%
100%
5.95
6
6.05
6.1
6.15
6.2
6.25
X (m)
×10^5

Figure 8

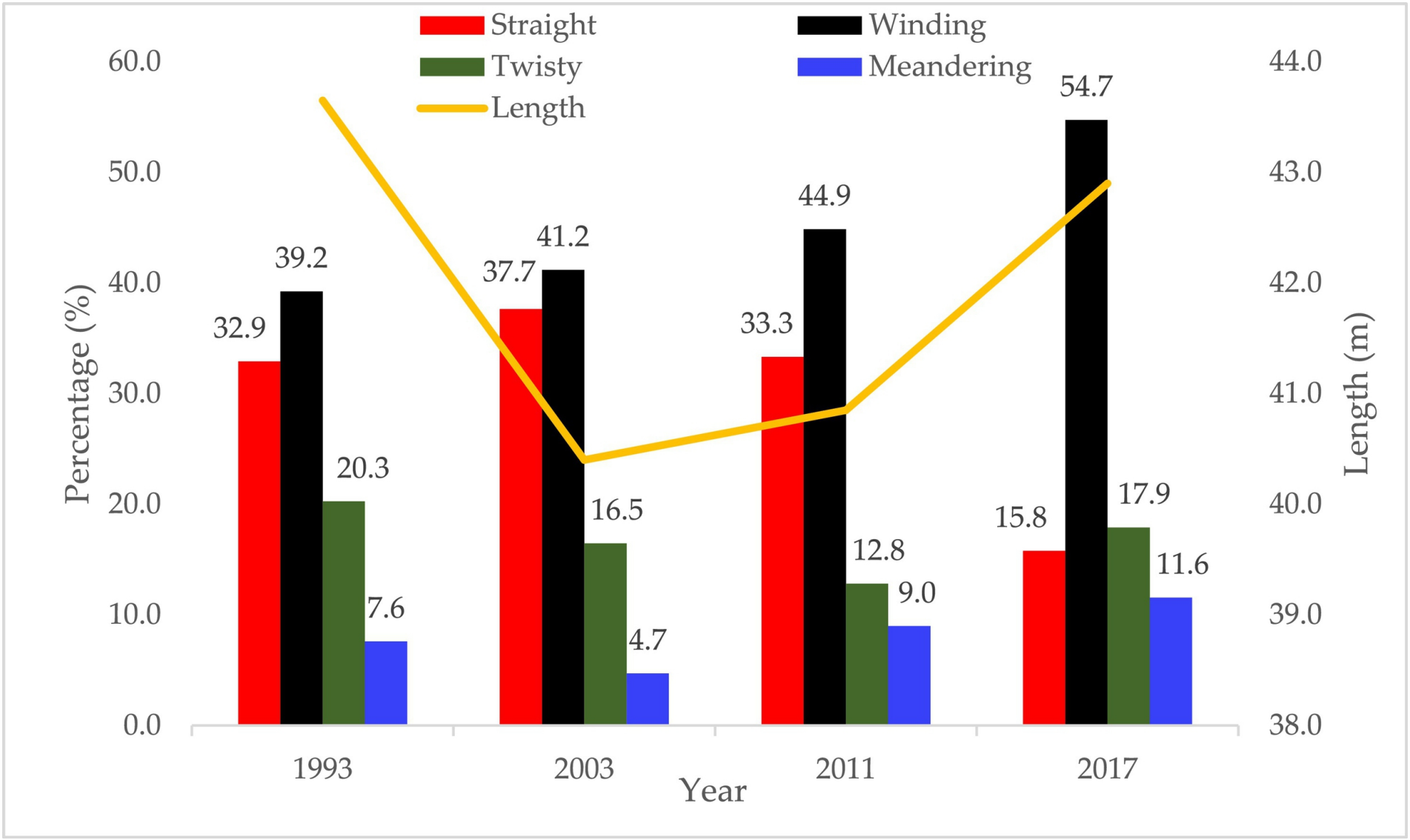
Straight
Winding
Twisty
Meandering
Length
60.0
50.0
40.0
30.0
20.0
10.0
0.0
Percentage (%)
44.0
43.0
42.0
41.0
40.0
39.0
38.0
Length (m)
32.9
39.2
20.3
7.6
37.7
41.2
16.5
4.7
33.3
44.9
12.8
9.0
15.8
54.7
17.9
11.6
1993
2003
2011
2017
Year

Figure 9

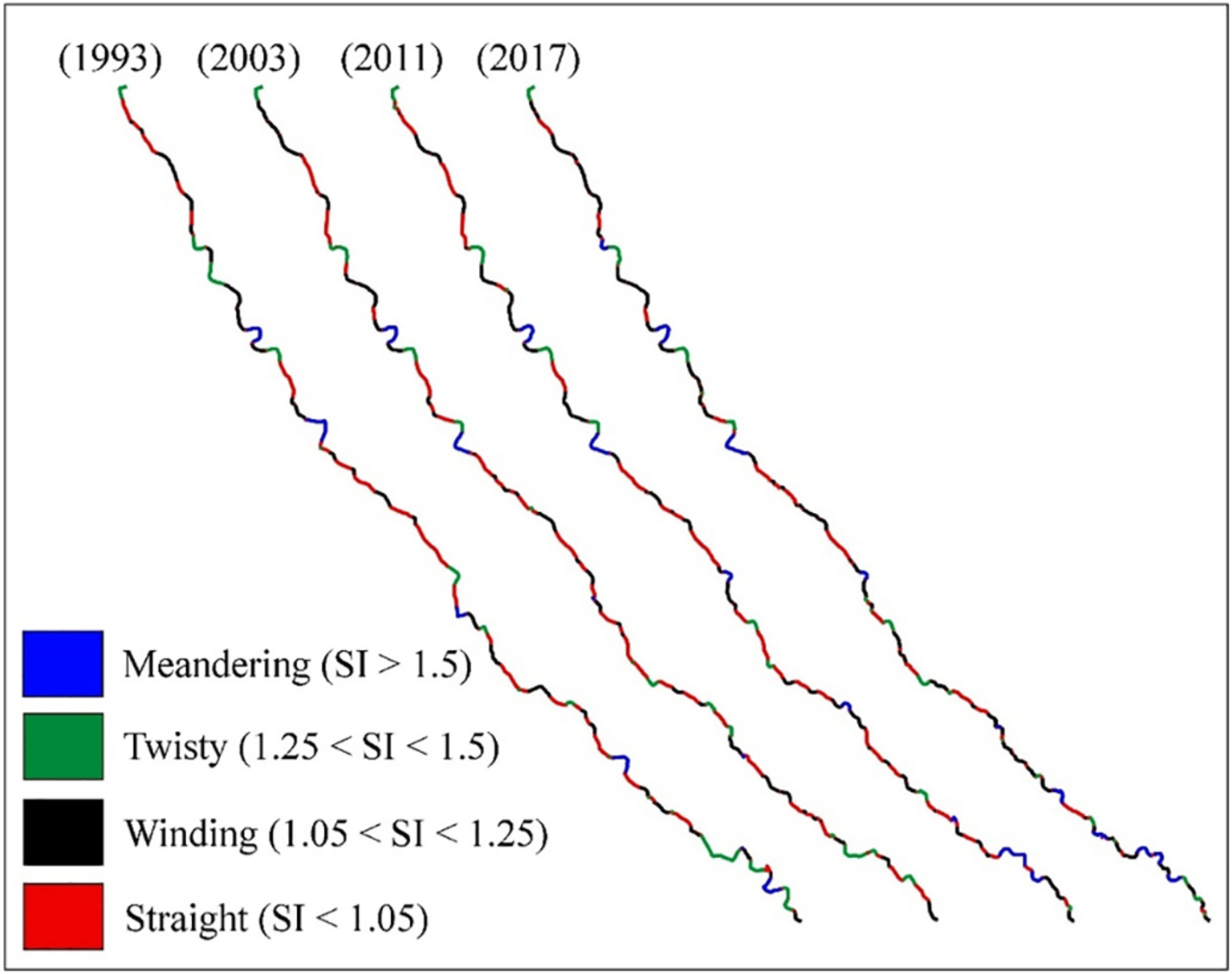
(1993)
(2003)
(2011)
(2017)
Meandering (SI > 1.5)
Twisty (1.25 < SI < 1.5)
Winding (1.05 < SI < 1.25)
Straight (SI < 1.05)

Figure 10

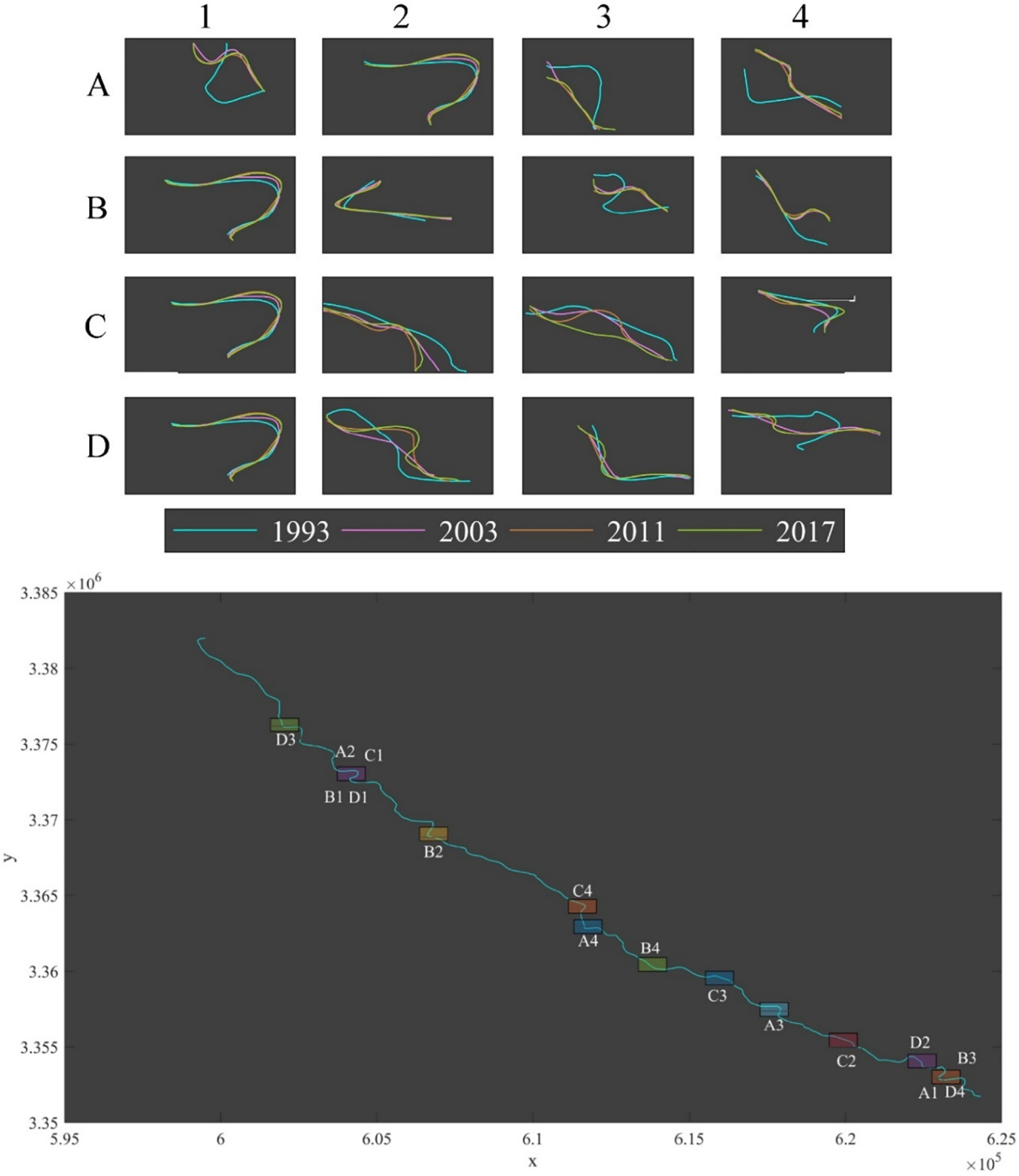
1
2
3
4
A
B
C
D
1993
2003
2011
2017
×10^6
3.385
3.38
3.375
3.37
3.365
3.36
3.355
3.35
y
D3
A2
C1
B1
D1
B2
C4
A4
B4
C3
A3
C2
D2
B3
A1
D4
5.95
6
6.05
6.1
6.15
6.2
6.25
x
×10^5

Figure 11

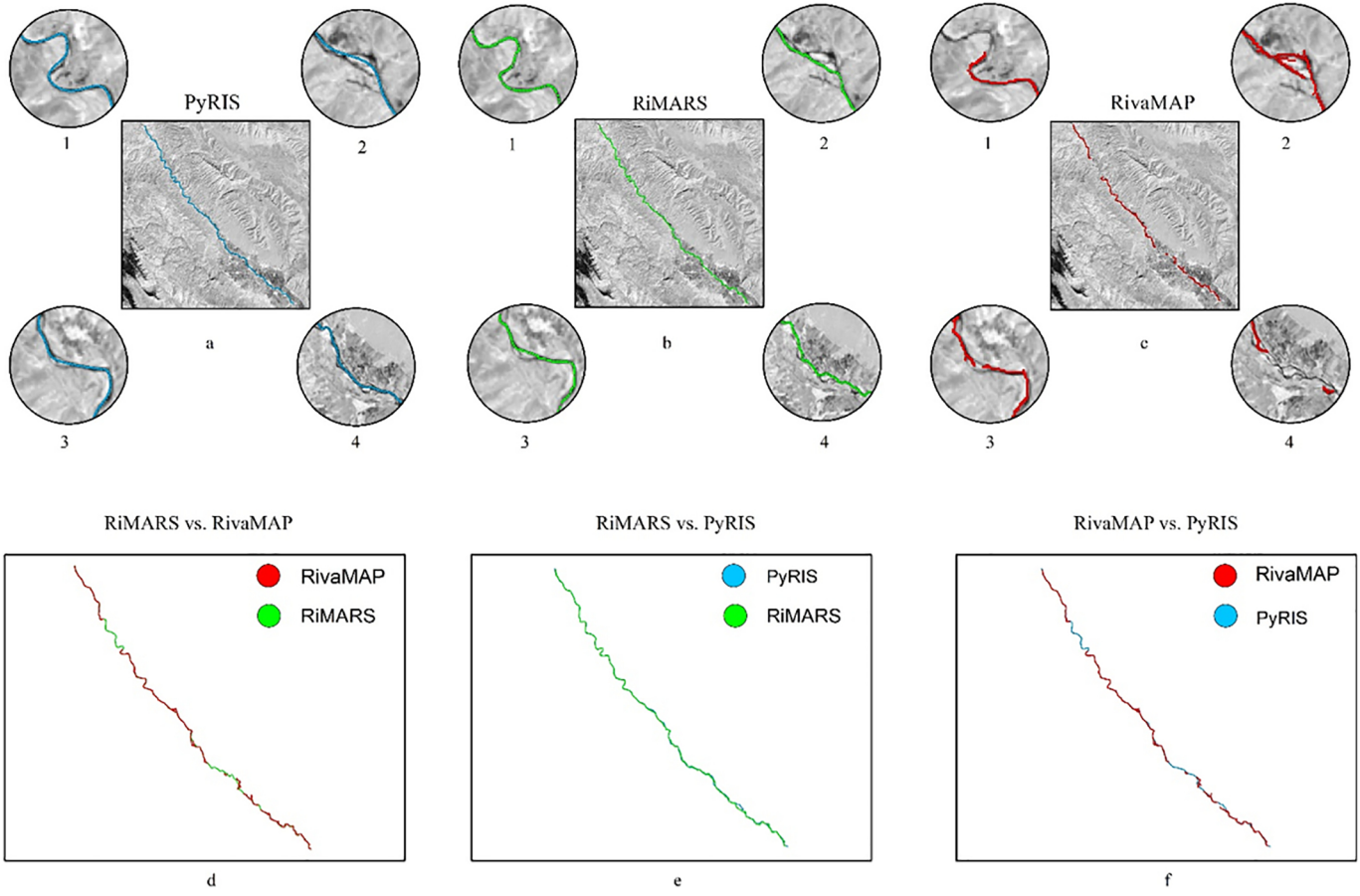
PyRIS
1
2
a
3
4
RiMARS
1
2
b
3
4
RivaMAP
1
2
c
3
4
RiMARS vs. RivaMAP
RivaMAP
RiMARS
d
RiMARS vs. PyRIS
PyRIS
RiMARS
e
RivaMAP vs. PyRIS
RivaMAP
PyRIS
f

Figure 12